Three-dimensional object recognition by Fourier transform profilometry

José J. Esteve-Taboada, David Mas, and Javier García

An automatic method for three-dimensional (3-D) shape recognition is proposed. It combines the Fourier transform profilometry technique with a real-time recognition setup such as the joint transform correlator (JTC). A grating is projected onto the object surface resulting in a distorted grating pattern. Since this pattern carries information about the depth and the shape of the object, their comparison provides a method for recognizing 3-D objects in real time. A two-cycle JTC is used for this purpose. Experimental results demonstrate the theory and show the utility of the new proposed method. © 1999 Optical Society of America

OCIS codes: 100.4550, 100.6890.

1. Introduction

Much research has been devoted to pattern recognition through optical correlation. Optical correlation has several advantages over digital methods, e.g., parallel and real-time processing abilities.

Most of the existing methods for pattern recognition have been developed for bidimensional (2-D) objects. The most frequently used optical correlators for this purpose have been the VanderLugt optical correlator[1] and the joint transform correlator (JTC).[2] Both are capable of performing 2-D optical correlation in real time, although the VanderLugt setup requires a holographic recording of the reference signal and must be accurately aligned with the optical axis. On the other hand, in the JTC setup the reference and the target are displayed side by side at the input plane, reducing the alignment requirements, and, moreover, there is no need for holographic recording.

In spite of the usefulness of 2-D pattern recognition, there are applications in which the object information is not contained in just one 2-D projection but in its whole three-dimensional (3-D) shape. Thus a full 3-D treatment is required. One simple approximation to the problem may consist of taking several planar projections of the scene and correlating them with their corresponding projections of the reference. This solution has been successfully applied in Ref. 3, but the huge amount of storage requirement and the complexity of designing a full reference signal make implementation of this technique complex.

An alternative solution was proposed in Ref. 4. In that paper a segmentation of connected planar and quadric surfaces of the object was used. The images were captured with a range camera and then digitally processed. A feed-forward neural network was then used to perform the final recognition task. Unfortunately, the required device for acquiring range images is not easily available, and the method needs a previous segmentation of the image.

Recently, Rosen proposed an electro-optical implementation of a 3-D spatial correlation (see Refs. 5 and 6). As an example of an application with his method, he described a 3-D JTC that is able to recognize targets in the 3-D space. The main drawback of the electro-optical setup is the need for massive digital calculation that may slow down the processing speed. This setup has the additional complexity of requiring an array of cameras for image acquisition.

On the other hand, several techniques have been devised for 3-D image acquisition.[7] In particular, in Ref. 8 a technique for automatic 3-D shape measurement is proposed and experimentally verified. This method, called Fourier transform profilometry (FTP), is based on projecting a grating on an object surface and capturing the resultant image with a CCD camera. The image obtained is a deformed grating pattern that carries information on the depth and the shape of the object. The image is digitally pro-

The authors are with Departament Interuniversitari d'Òptica, Facultat de Física, Universitat de València, C/Doctor Moliner 50, 46100 Burjassot, València, Spain. J. J. Esteve-Taboada's e-mail address is jose.j.esteve@uv.es.

Received 7 January 1999; revised manuscript 15 April 1999.
0003-6935/99/224760-06$15.00/0

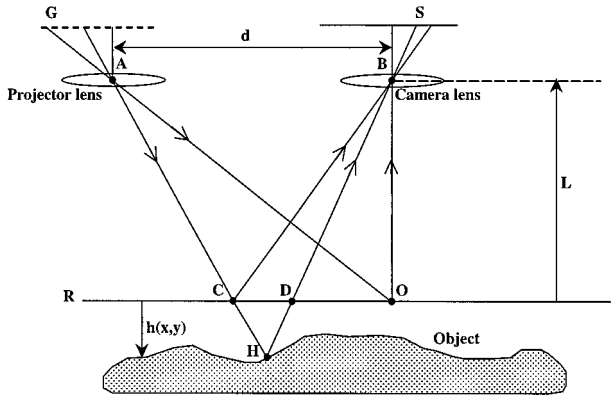

Fig. 1. Optical arrangement for projecting the grating and grabbing the input image.

cessed. and a final 3-D image is obtained. It must be taken into account that for proper application of the method the spatial frequencies of the objects (considering reflectivity and the 3-D shape) should be small compared with the frequency of the projected grating, i.e., only relatively smooth objects can be analyzed.

Since the deformed fringe pattern obtained with the FTP technique carries information about the complete shape of the object, a comparison of such patterns with a reference pattern will provide a method for recognizing 3-D objects. In this paper we prove this statement and design an optical setup that will perform the detection in real time. The recognition task is based on the 3-D shape of the object and not only on its 2-D profile. For this purpose, we use a modified JTC setup that offers clear advantages in practical implementations with respect to a VanderLugt correlator because it is not likely to be optically misaligned and it is easy to construct.[9]

In Section 2 we review the main aspects of the FTP method introduced in Ref. 8 that are relevant for our purposes. In Section 3 we apply the mathematics derived in Section 2 to our particular case: the 3-D JTC. In Section 4 optical experiments show the utility of the method introduced here. Finally, in Section 5 the main conclusions are outlined.

2. Fourier Transform Profilometry Method

Two different optical geometries have been proposed in the FTP method.[8] In our experiment we employ the parallel-optical-axes geometry (see Fig. 1) in which the optical axes of a projector and a camera lie in the same plane and are parallel. Let us consider a reference plane R, which is a fictitious plane that serves as a reference from which the object height $h(x, y)$ is measured. The lines of grating G are normal to the plane of the figure, and the projector lens forms its conjugate image (with period p) on plane R. The reference plane is imaged onto sensor plane S by the camera lens. When the object is a flat surface on R, i.e., $h(x, y) = 0$, the grating image projected onto the object surface is a regular pattern that can be expressed by its Fourier series expansion:

$$g_0(x, y) = \sum_{n=-\infty}^{\infty} A_n \exp(2\pi i n f_0 x), \tag{1}$$

where

$$f_0 = \frac{1}{p} \tag{2}$$

is the fundamental frequency of the observed grating image. For a general object with varying $h(x, y)$ the deformed grating image is given by

$$g(x, y) = r(x, y) \sum_{n=-\infty}^{\infty} A_n \exp\{2\pi i n f_0[x + s(x, y)]\}, \tag{3}$$

where $r(x, y)$ is the reflectivity distribution on the object surface [$r(x, y)$ is zero outside the object extent] and $s(x, y) = \overline{CD}$ in Fig. 1. We can express this equation as a spatially phase-modulated signal

$$g(x, y) = r(x, y) \sum_{n=-\infty}^{\infty} A_n \exp\{i[2\pi n f_0 x + n\phi(x, y)]\}, \tag{4}$$

where

$$\phi(x, y) = 2\pi f_0 s(x, y) = 2\pi f_0 \overline{CD}. \tag{5}$$

This deformed grating [see Eq. (4)] can be interpreted in terms of its diffraction orders, each with a spatial carrier frequency nf_0 modulated in phase through $n\phi(x, y)$ and with an overall amplitude modulation $r(x, y)$. For future use we rewrite Eq. (4), separating the phase terms as

$$g(x, y) = r(x, y) \sum_{n=-\infty}^{\infty} q_n(x, y)\exp(2\pi i n f_0 x), \tag{6}$$

where

$$q_n(x, y) = A_n \exp[in\phi(x, y)]. \tag{7}$$

To obtain a connection between the phase $\phi(x, y)$ and the height $h(x, y)$, we note that ΔAHB is similar to ΔCHD; therefore we can write

$$\overline{CD} = \frac{-dh(x, y)}{L - h(x, y)}, \tag{8}$$

and thus, following Eq. (5), we have

$$\phi(x, y) = \frac{-2\pi f_0 dh(x, y)}{L - h(x, y)}. \tag{9}$$

We can see here that the phase $\phi(x, y)$ contains information about the 3-D shape to be measured.

If the camera and the projector are far from the object, at the denominator of Eq. (9) $h(x, y)$ can be neglected with respect to L, and thus $\phi(x, y) \simeq kh(x, y)$, k being a constant equal to $-2\pi f_0 d/L$. Recalling Eq. (7), the amplitude in any order n of the Fourier expansion of the distorted grating has the form

$$r(x, y)q_n(x, y) \simeq r(x, y)A_n \exp[inkh(x, y)], \tag{10}$$

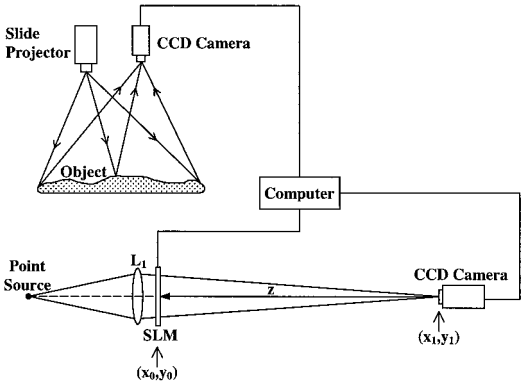

Fig. 2. Experimental setup including the acquisition part and the JTC process.

so the phase of every order $q_n(x, y)$ is proportional to the height of the object.

In general, the condition $L \gg h(x, y)$ is not necessary for our purpose. We can obtain the phase of every order by using Eq. (9). As we see below, this method provides a final equation that carries information about the similar 3-D shape of the objects to be checked. Therefore the height of the 3-D object has been encoded as a phase function either linearly or by a more complicated relation given by Eq. (9).

3. Three-Dimensional Joint Transform Correlator

In this section we apply the mathematics derived in Section 2 to our particular case: the 3-D JTC.

Consider that we project a regular grating pattern on some 3-D objects to be checked for recognition and we take the image of these objects with a camera. We obtain some distorted grating patterns that carry information about the 3-D shape of the objects, so that, comparing these patterns, we can recognize a particular 3-D object. To compare the 3-D shapes, we use a modified JTC (see Fig. 2). This setup contains a spatial light modulator (SLM) at the input plane (x_0, y_0), which will display the deformed grating patterns. This SLM is illuminated with a convergent beam obtained with lens L_1, so that we have the Fourier transform of the input function at plane (x_1, y_1). If we take the intensity distribution at this plane and put it at the SLM plane again, we obtain a correlation image at plane (x_1, y_1) that permits us to compare the 3-D input shapes.

Let us suppose two input objects at the reference plane described by their heights $h(x, y)$ and $h'(x, y)$. These objects are centered, for example, at positions $(0, Y/2)$ and $(0, -Y/2)$, respectively [see Fig. 3(a)]. The distorted grating patterns can be described by two functions, $s(x, y)$ and $s'(x, y)$ [see Fig. 3(b)]. The image of the distorted grating patterns is grabbed by the CCD camera and fed to the SLM,

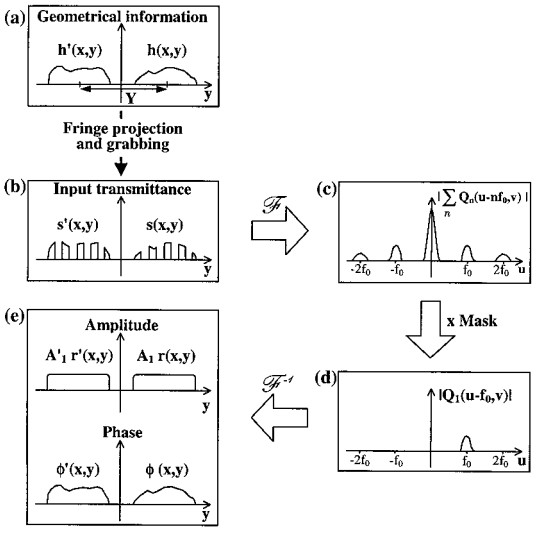

Fig. 3. Scheme of the procedure for obtaining object-height information by fringe projection. For simplicity a linear phase factor has been removed in (e), and the objects are assumed to have uniform reflectivity.

providing an amplitude at the input plane (x_0, y_0) given by

$$U_0(x_0, y_0) = s(x_0, y_0 - Y/2) + s'(x_0, y_0 + Y/2), \quad (11)$$

where, following Eq. (6), functions $s(x_0, y_0)$ and $s'(x_0, y_0)$ are given by

$$s(x_0, y_0) = r(x_0, y_0) \sum_{n=-\infty}^{\infty} q_n(x_0, y_0)\exp(2\pi i n f_0 x_0), \quad (12)$$

$$s'(x_0, y_0) = r'(x_0, y_0) \sum_{n=-\infty}^{\infty} q_n'(x_0, y_0)\exp(2\pi i n f_0 x_0). \quad (13)$$

At plane (x_1, y_1) we have the 2-D Fourier transform of $U_0(x_0, y_0)$ with the scaling given by λz [z being the distance from plane (x_1, y_1) to plane (x_0, y_0) and λ the wavelength of illumination]. The complex amplitude at plane (x_1, y_1) can be written as

$$U_1(x_1, y_1) = S\left(\frac{x_1}{\lambda z}, \frac{y_1}{\lambda z}\right)\exp(-i\pi y_1 Y/\lambda z) + S'\left(\frac{x_1}{\lambda z}, \frac{y_1}{\lambda z}\right)\exp(i\pi y_1 Y/\lambda z), \quad (14)$$

where S and S' represent the 2-D Fourier transforms of s and s', respectively. In Eq. (14) we have dropped a $1/i\lambda z$ factor and a global quadratic phase factor (see Ref. 10, for example), which is irrelevant for our purposes since we consider only the intensity of the distribution. Changing the distance between the SLM and the CCD camera allows for Fourier transform scaling to fit the area of the CCD. Real optical systems will also introduce the effect of limited apertures, which has been neglected in our treatment (see also Ref. 10 for more details).

The 2-D Fourier transform for the $s(x_0, y_0)$ function can be expressed as

$$S\left(\frac{x_1}{\lambda z}, \frac{y_1}{\lambda z}\right) = S(u, v) = \left[\sum_{n=-\infty}^{\infty} Q_n(u - nf_0, v)\right] \otimes \mathcal{F}[r(x_0, y_0)], \tag{15}$$

with $Q_n(u, v)$ being the Fourier transform of $q_n(x_0, y_0)$. The symbol $\otimes$ denotes the convolution operation. A similar expression holds for the 2-D Fourier transform of $s'(x_0, y_0)$.

Therefore Eq. (14) may be rewritten [taking into account that $u = (x_1/\lambda z)$ and $v = (y_1/\lambda z)$] as

$$U_1(u, v) = \left\{\left[\sum_{n=-\infty}^{\infty} Q_n(u - nf_0, v)\right] \otimes \mathcal{F}[r(x_0, y_0)]\right\} \times \exp\{-i\pi vY\} + \left\{\left[\sum_{n=-\infty}^{\infty} Q_n'(u - nf_0, v)\right] \otimes \mathcal{F}[r'(x_0, y_0)]\right\}\exp(i\pi vY). \tag{16}$$

Assuming that $r(x, y)[r'(x, y)]$ and $\phi(x, y)[\phi'(x, y)]$ vary slowly compared with the frequency f_0 of the grating pattern, we can consider that all the spectra $Q_n(u - nf_0, v)[Q_n'(u - nf_0, v)]$ are separated from one another by carrier frequency f_0 [see Fig. 3(c)], so that, using a mask at plane (x_1, y_1), we can easily filter these spectra and select only the spectrum with $n = 1$ [see Fig. 3(d)]:

$$U_1'(u, v) = \{Q_1(u - f_0, v) \otimes \mathcal{F}[r(x_0, y_0)]\} \times \exp(-i\pi vY) + \{Q_1'(u - f_0, v) \otimes \mathcal{F}[r'(x_0, y_0)]\}\exp(i\pi vY). \tag{17}$$

The object-height information can be obtained as an encoded phase modulation with an inverse Fourier transform of Eq. (17):

$$\mathcal{F}^{-1}[U_1'(u, v)] = A_1 r(x_1, y_1)\exp\{i[\phi(x_1, y_1) + 2\pi f_0 x_1]\} \otimes \delta(x_1, y_1 - Y/2) + A_1' r'(x_1, y_1)\exp\{i[\phi'(x_1, y_1) + 2\pi f_0 x_1]\} \otimes \delta(x_1, y_1 + Y/2). \tag{18}$$

Equation (18) has two complex terms. Figure 3(e) depicts a simplified example of these two terms separating the amplitude and the phase information. As stated in Section 2, the phase, aside from a linear phase factor, contains the object-height information. The delta functions locate the patterns in their original locations.

Nevertheless, to obtain for pattern-recognition purposes a comparison between these phase-modulated functions, we go on with the modified JTC setup. This allows for skipping this phase extraction and dealing with only the Fourier domain. Therefore we now take the intensity of $U_1'(u, v)$ [this is at the first diffraction order at plane (x_1, y_1)] with a second camera (see Fig. 2):

$$I(u, v) = |Q_1(u - f_0, v) \otimes \mathcal{F}[r(x_0, y_0)]|^2 + |Q_1'(u - f_0, v) \otimes \mathcal{F}[r'(x_0, y_0)]|^2 + \{Q_1(u - f_0, v) \otimes \mathcal{F}[r(x_0, y_0)]\}(Q_1'^*(u - f_0, v) \otimes \{\mathcal{F}[r'(x_0, y_0)]\}^*)\exp(-i2\pi vY) + (Q_1^*(u - f_0, v) \otimes \{\mathcal{F}[r(x_0, y_0)]\}^*)\{Q_1'(u - f_0, v) \otimes \mathcal{F}[r'(x_0, y_0)]\}\exp(i2\pi vY), \tag{19}$$

where the asterisk indicates the complex conjugate operation.

This image is sent again to the SLM at plane (x_0, y_0). The new field at plane (x_1, y_1) will be the Fourier transform of the function $I(u, v)$. Taking into account the scaling factors and coordinate inversions, this new field distribution results in

$$U_2(x_1, y_1) = \tilde{s}(x_1, y_1) \star \tilde{s}(x_1, y_1) + \tilde{s}'(x_1, y_1) \star \tilde{s}'(x_1, y_1) + [\tilde{s}(x_1, y_1) \star \tilde{s}'(x_1, y_1)] \otimes \delta(x_1, y_1 - Y) + [\tilde{s}'(x_1, y_1) \star \tilde{s}(x_1, y_1)] \otimes \delta(x_1, y_1 + Y), \tag{20}$$

where the star symbol $\star$ denotes the cross-correlation operation, and functions $\tilde{s}(x_1, y_1)$ and $\tilde{s}'(x_1, y_1)$ are

$$\tilde{s}(x_1, y_1) = r(-x_1, -y_1)q_1(-x_1, -y_1)\exp(-2\pi i f_0 x_1) = r(-x_1, -y_1)A_1\exp\{i[\phi(-x_1, -y_1) - 2\pi f_0 x_1]\}, \tag{21}$$

$$\tilde{s}'(x_1, y_1) = r'(-x_1, -y_1)A_1'\exp\{i[\phi'(-x_1, -y_1) - 2\pi f_0 x_1]\}. \tag{22}$$

In the expression for $U_2(x_1, y_1)$ given by Eq. (20) the third and the fourth terms are the cross correlations between functions $\tilde{s}$ and $\tilde{s}'$. The third is centered at coordinates $(0, Y)$ and the fourth at coordinates $(0, -Y)$. One is a mirror reflection of the other about the optical axis. This analysis is also valid if instead of a second object $s'(x, y)$ we have a scene [say, $f(x, y)$] composed of several objects. In fact, this is the most common case in the applications in which an object has to be recognized in a complex scene. Therefore in the upper part of the output plane the correlation between the scene $f(x, y)$ and the reference $s(x, y)$ will be obtained.

Going back to the analysis of Eq. (20), we can see immediately that the cross correlation between functions $\tilde{s}(x_1, y_1)$ and $\tilde{s}'(x_1, y_1)$,

$$\tilde{s}(x_1, y_1) \star \tilde{s}'(x_1, y_1) = \iint_{-\infty}^{\infty} \tilde{s}(\alpha, \beta)\tilde{s}'^*(\alpha - x_1, \beta - y_1)d\alpha d\beta = A_1 A_1'^* \exp(-2\pi i f_0 x_1)\{r(x_1, y_1) \times \exp[i\phi(x_1, y_1)] \star r'(x_1, y_1) \times \exp[i\phi'(x_1, y_1)]\}, \tag{23}$$

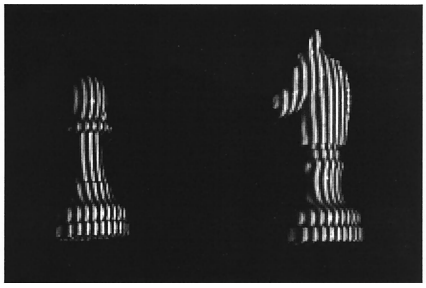

(a)

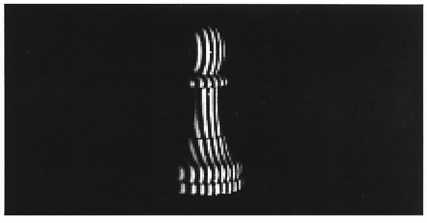

(b)

Fig. 4. (a) Input scene. (b) Reference object. Both images are displayed side by side on the SLM. Note that, despite the 3-D shapes of the two pawns being the same, the deformed grating pattern is different, owing to the different location of the grating.

carries information about the similar 3-D shape of the $s(x_0, y_0)$ and $s'(x_0, y_0)$ functions. This cross-correlation function contains a correlation between $r(x_1, y_1)\exp[i\phi(x_1, y_1)]$ and $r'(x_1, y_1)\exp[i\phi'(x_1, y_1)]$, where r and r' are the reflectivity distributions and ϕ and ϕ' contain the object-height information encoded as a phase modulation [see Eq. (9)].

Note that, if the camera and the projector are far from the object, i.e., $L \gg h(x, y)$, our experimental setup is invariant to shifts along the direction given by $h(x, y)$. This can be checked in Eq. (10): Any constant added to height $h(x, y)$ would appear in Eq. (23) like another constant affecting the whole correlation.

Therefore we are able to detect similar 3-D shapes by comparing the filtered distorted fringe patterns obtained when we project a grating on some 3-D objects. Finally, note that Eq. (23) is the correlation between the phase-encoded 3-D input objects and not that between the fringe patterns themselves. This correlation allows detection that is invariant under displacements on the three axes. This is in contrast with other approaches in which the fringes are used to make the correlation process spatially variant.[11]

4. Experimental Results

The usefulness of the method has been tested by an optical experiment. The actual setup is the one shown in Fig. 2. The parallel-optical-axes geometry is used for fringe projection. A slide projector is used to image a Ronchi grating of 8 lines/mm onto the objects' surface. The objects are three chess pieces (two pawns and a knight) placed in a black uniform plane that serves as a reference from which object heights are compared. One of the pawns is the reference object, while the other pawn and the knight

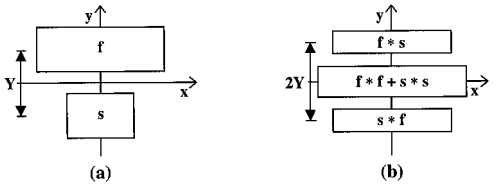

Fig. 5. (a) Input plane arrangement for the input scene f and the reference object s. (b) Output plane of the JTC. The asterisk indicates the cross-correlation operation.

serve as the input image to be analyzed. The effect of using a different grating profile (sinusoidal, for example), according to the theory in Section 2, would change our expression in only a global amplitude factor (the Fourier coefficient of the selected order in the Fourier domain).

The deformed grating patterns are recorded by a Pulnix Model TM-765 CCD camera. This video frame is composed of two parts: the upper part is the input scene [see Fig. 4(a)], and the lower part is the object to be detected [see Fig. 4(b)]. As can be observed in the images, although the 3-D shape of the two pawns is the same, the deformed grating pattern is different, owing to the different location of the grating. The video output signal is stored in a frame-grabber memory as a 256×256 pixel image containing an arrangement like the one shown in Fig. 5(a). This digital image is sent to the SLM at plane (x_0, y_0) of the optical setup (see Fig. 2). The SLM is a liquid-crystal screen obtained from an Epson Model VP-100PS video projector. L_1 is a Nikon 135-mm $f/2$ photographic lens.

With a second Pulnix CCD camera without a lens the intensity of the first order at plane (x_1, y_1) is obtained. This image is sent to the SLM again. Therefore, as shown above, in this new cycle of the modified JTC we have finally at plane (x_1, y_1) correlation terms in three different positions. Following Eq. (20), in the optical axis we will obtain the addition of the autocorrelation terms; in the upper part of the

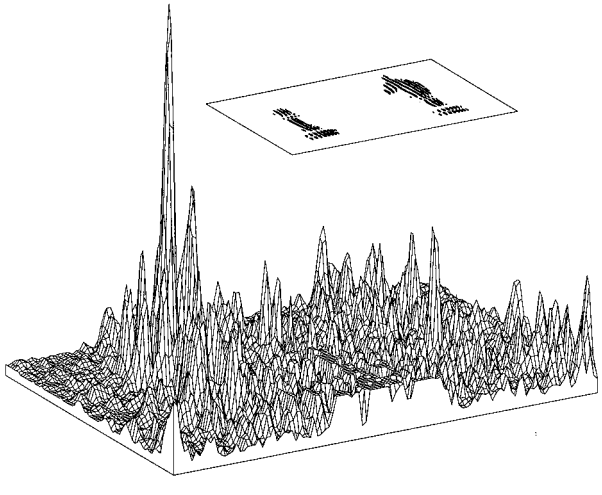

Fig. 6. Experimental optical correlation. The zero order in the lowest part of the image has been clipped for graphic purposes.

image we will obtain the correlation between the input scene and the reference object, and in the lower part we will obtain the same distribution except for a mirror reflection [see Fig. 5(b)]. This output plane is captured again with a CCD camera, so the intensity of this distribution is recorded. Figure 6 shows the experimentally obtained intensity output plane when the input objects are the chess pieces shown in Fig. 4(a). This plot shows only the upper part of the JTC output, containing only the correlation term between the input scene and the target. This correlation output takes into account the information about the similarity of the 3-D shape of the objects. Aside from the zero order in the lowest part of the image, which has been clipped for graphic purposes, we can observe a high correlation peak owing to the pawn appearing in the input scene. This peak allows a clear discrimination with the cross-correlation term that appears at the right part of the image owing to the knight. Note that we made no effort to enhance the experimental correlation peak further (see, for example, image-processing algorithms or nonlinear processing applied to the Fourier domain in Refs. 12 and 13, respectively).

5. Conclusions

We have presented a novel method for achieving 3-D shape detection. The method is based on using 3-D information contained in the deformed fringe pattern obtained when a grating is projected onto the objects' surface. When this deformed fringe pattern is analyzed, it has been shown that the first order of its Fourier series expansion contains the objects' height information encoded on the phase. Therefore taking the intensity of the first diffraction order permits the realization of a modified JTC recognition process in which the input function is the distorted pattern that contains the 3-D shape of the objects with a phase-encoded height.

The proposed method has been optically implemented by a two-cycle JTC. In the first cycle the intensity at the first diffraction order of the deformed fringe pattern is taken and sent again to the JTC input plane. The output of the second cycle contains the desired correlation. Our system inherits from linear correlation the invariance to translations in a plane perpendicular to the line of sight; moreover, in certain conditions our setup is invariant to shifts along the direction given by the height of the object. The procedure also takes from linear correlation the sensitivity to distortions of the object. Changes in the 3-D orientation of the object will result in different height information, degrading the correlation output.

Experimental results verify the derived theory and show the utility of the method introduced here. The whole experimental setup can be constructed with simple equipment, and, except for grabbing the images, there is no need for electronic or digital processing. As a consequence the system is simple and robust. Moreover, the system can operate at nearly video rates. The fully real-time feature is lost, because in our actual system we need an enabled and a disabled binary mask for selection of the first-order spectrum. Although this procedure is fast, it requires a certain processing time. Alternatively, a fully real-time setup could be done by cascading another optical Fourier transform line by using the masked intensity signal for driving another SLM in the second Fourier transform line. Coordinate inversion produced by two consecutive Fourier transforms could be avoided by suitably addressing the SLM. In this case the speed would be limited only by the speeds of the SLM and the camera, usually operating at video rates.

José J. Esteve-Taboada acknowledges a grant from Conselleria de Cultura, Educació i Ciència (Generalitat Valenciana). This research has been partially supported by the Spanish Ministerio de Educación y Cultura under project PB96-1134-C02-02.

References

1. A. VanderLugt, "Signal detection by complex spatial filtering," IEEE Trans. Inf. Theory **IT-10,** 139–145 (1964).
2. C. S. Weaver and J. W. Goodman, "A technique for optically convolving two functions," Appl. Opt. **5,** 1248–1249 (1966).
3. A. Pu, R. Denkewalter, and D. Psaltis, "Real-time vehicle navigation using a holographic memory," Opt. Eng. **36,** 2737–2746 (1997).
4. E. Paquet, M. Rioux, and H. H. Arsenault, "Invariant pattern recognition for range images using the phase Fourier transform and a neural network," Opt. Eng. **34,** 1178–1183 (1995).
5. J. Rosen, "Three-dimensional electro-optical correlation," J. Opt. Soc. Am. A **15,** 430–436 (1998).
6. J. Rosen, "Three-dimensional joint transform correlator," Appl. Opt. **37,** 7538–7544 (1998).
7. O. Faugeras, *Three-Dimensional Computer Vision. A Geometric Viewpoint* (MIT Press, Cambridge, Mass., 1993).
8. M. Takeda and K. Mutoh, "Fourier transform profilometry for the automatic measurement of 3-D object shapes," Appl. Opt. **22,** 3977–3982 (1983).
9. X. J. Lu, F. T. S. Yu, and D. A. Gregory, "Comparison of VanderLugt and joint transform correlators," Appl. Phys. B **51,** 153–164 (1990).
10. J. W. Goodman, *Introduction to Fourier Optics,* Physical and Quantum Electronics Series (McGraw-Hill, New York, 1968).
11. T. Haist, M. Schönleber, and H. J. Tiziani, "Positioning of noncooperative objects by use of joint transform correlation combined with fringe projection," Appl. Opt. **37,** 7553–7559 (1998).
12. M. Alam and Y. Gu, "Sobel operator based multiobject joint transform correlation," Optik (Stuttgart) **100,** 28–32 (1995).
13. B. Javidi, "Nonlinear joint power spectrum based optical correlation," Appl. Opt. **28,** 2358–2367 (1989).